Chemostratigraphy Across Major Chronological Boundaries

Alcides N. Sial, Claudio Gaucher, Muthuvairavasamy Ramkumar, and Valderez Pinto Ferreira

Editors

AGU100 ADVANCING EARTH AND SPACE SCIENCE

WILEY

Geophysical Monograph Series

189 **Climate Dynamics: Why Does Climate Vary?** *De-Zheng Sun and Frank Bryan (Eds.)*
190 **The Stratosphere: Dynamics, Transport, and Chemistry** *L. M. Polvani, A. H. Sobel, and D. W. Waugh (Eds.)*
191 **Rainfall: State of the Science** *Firat Y. Testik and Mekonnen Gebremichael (Eds.)*
192 **Antarctic Subglacial Aquatic Environments** *Martin J. Siegert, Mahlon C. Kennicut II, and Robert A. Bindschadler (Eds.)*
193 **Abrupt Climate Change: Mechanisms, Patterns, and Impacts** *Harunur Rashid, Leonid Polyak, and Ellen Mosley-Thompson (Eds.)*
194 **Stream Restoration in Dynamic Fluvial Systems: Scientific Approaches, Analyses, and Tools** *Andrew Simon, Sean J. Bennett, and Janine M. Castro (Eds.)*
195 **Monitoring and Modeling the Deepwater Horizon Oil Spill: A Record-Breaking Enterprise** *Yonggang Liu, Amy MacFadyen, Zhen-Gang Ji, and Robert H. Weisberg (Eds.)*
196 **Extreme Events and Natural Hazards: The Complexity Perspective** *A. Surjalal Sharma, Armin Bunde, Vijay P. Dimri, and Daniel N. Baker (Eds.)*
197 **Auroral Phenomenology and Magnetospheric Processes: Earth and Other Planets** *Andreas Keiling, Eric Donovan, Fran Bagenal, and Tomas Karlsson (Eds.)*
198 **Climates, Landscapes, and Civilizations** *Liviu Giosan, Dorian Q. Fuller, Kathleen Nicoll, Rowan K. Flad, and Peter D. Clift (Eds.)*
199 **Dynamics of the Earth's Radiation Belts and Inner Magnetosphere** *Danny Summers, Ian R. Mann, Daniel N. Baker, and Michael Schulz (Eds.)*
200 **Lagrangian Modeling of the Atmosphere** *John Lin (Ed.)*
201 **Modeling the Ionosphere-Thermosphere** *Jospeh D. Huba, Robert W. Schunk, and George V. Khazanov (Eds.)*
202 **The Mediterranean Sea: Temporal Variability and Spatial Patterns** *Gian Luca Eusebi Borzelli, Miroslav Gacic, Piero Lionello, and Paola Malanotte-Rizzoli (Eds.)*
203 **Future Earth – Advancing Civic Understanding of the Anthropocene** *Diana Dalbotten, Gillian Roehrig, and Patrick Hamilton (Eds.)*
204 **The Galápagos: A Natural Laboratory for the Earth Sciences** *Karen S. Harpp, Eric Mittelstaedt, Noémi d'Ozouville, and David W. Graham (Eds.)*
205 **Modeling Atmospheric and Oceanic Flows: Insightsfrom Laboratory Experiments and Numerical Simulations** *Thomas von Larcher and Paul D. Williams (Eds.)*
206 **Remote Sensing of the Terrestrial Water Cycle** *Venkat Lakshmi (Ed.)*
207 **Magnetotails in the Solar System** *Andreas Keiling, Caitríona Jackman, and Peter Delamere (Eds.)*
208 **Hawaiian Volcanoes: From Source to Surface** Rebecca *Carey, Valerie Cayol, Michael Poland, and Dominique Weis (Eds.)*
209 **Sea Ice: Physics, Mechanics, and Remote Sensing** *Mohammed Shokr and Nirmal Sinha (Eds.)*
210 **Fluid Dynamics in Complex Fractured-Porous Systems** *Boris Faybishenko, Sally M. Benson, and John E. Gale (Eds.)*
211 **Subduction Dynamics: From Mantle Flow to Mega Disasters** *Gabriele Morra, David A. Yuen, Scott King, Sang Mook Lee, and Seth Stein (Eds.)*
212 **The Early Earth: Accretion and Differentiation** *James Badro and Michael Walter (Eds.)*
213 **Global Vegetation Dynamics: Concepts and Applications in the MC1 Model** *Dominique Bachelet and David Turner (Eds.)*
214 **Extreme Events: Observations, Modeling and Economics** *Mario Chavez, Michael Ghil, and Jaime Urrutia-Fucugauchi (Eds.)*
215 **Auroral Dynamics and Space Weather** *Yongliang Zhang and Larry Paxton (Eds.)*
216 **Low-Frequency Waves in Space Plasmas** *Andreas Keiling, Dong-Hun Lee, and Valery Nakariakov (Eds.)*
217 **Deep Earth: Physics and Chemistry of the Lower Mantle and Core** *Hidenori Terasaki and Rebecca A. Fischer (Eds.)*
218 **Integrated Imaging of the Earth: Theory and Applications** *Max Moorkamp, Peter G. Lelievre, Niklas Linde, and Amir Khan (Eds.)*
219 **Plate Boundaries and Natural Hazards** *Joao Duarte and Wouter Schellart (Eds.)*
220 **Ionospheric Space Weather: Longitude and Hemispheric Dependences and Lower Atmosphere Forcing Timothy Fuller-Rowell**, *Endawoke Yizengaw, Patricia H. Doherty, and Sunanda Basu (Eds.)*
221 **Terrestrial Water Cycle and Climate Change Natural and Human-Induced Impacts** *Qiuhong Tang and Taikan Oki (Eds.)*
222 **Magnetosphere-Ionosphere Coupling in the Solar System** *Charles R. Chappell, Robert W. Schunk, Peter M. Banks, James L. Burch, and Richard M. Thorne (Eds.)*
223 **Natural Hazard Uncertainty Assessment: Modeling and Decision Support** *Karin Riley, Peter Webley, and Matthew Thompson (Eds.)*
224 **Hydrodynamics of Time-Periodic Groundwater Flow: Diffusion Waves in Porous Media** *Joe S. Depner and Todd C. Rasmussen (Auth.)*
225 **Active Global Seismology** *Ibrahim Cemen and Yucel Yilmaz (Eds.)*
226 **Climate Extremes** *Simon Wang (Ed.)*
227 **Fault Zone Dynamic Processes** *Marion Thomas (Ed.)*
228 **Flood Damage Survey and Assessment: New Insights from Research and Practice** *Daniela Molinari, Scira Menoni, and Francesco Ballio (Eds.)*
229 **Water-Energy-Food Nexus – Principles and Practices** *P. Abdul Salam, Sangam Shrestha, Vishnu Prasad Pandey, and Anil K Anal (Eds.)*
230 **Dawn–Dusk Asymmetries in Planetary Plasma Environments** *Stein Haaland, Andrei Rounov, and Colin Forsyth (Eds.)*
231 **Bioenergy and Land Use Change** *Zhangcai Qin, Umakant Mishra, and Astley Hastings (Eds.)*
232 **Microstructural Geochronology: Planetary Records Down to Atom Scale** *Desmond Moser, Fernando Corfu, James Darling, Steven Reddy, and Kimberly Tait (Eds.)*
233 **Global Flood Hazard: Applications in Modeling, Mapping and Forecasting** *Guy Schumann, Paul D. Bates, Giuseppe T. Aronica, and Heiko Apel (Eds.)*
234 **Pre-Earthquake Processes: A Multidisciplinary Approach to Earthquake Prediction Studies** *Dimitar Ouzounov, Sergey Pulinets, Katsumi Hattori, and Patrick Taylor (Eds.)*
235 **Electric Currents in Geospace and Beyond** *Andreas Keiling, Octav Marghitu, and Michael Wheatland (Eds.)*
236 **Quantifying Uncertainty in Subsurface Systems** *Céline Scheidt, Lewis Li and Jef Caers (Eds.)*
237 **Petroleum Engineering** *Moshood Sanni (Ed.)*
238 **Geological Carbon Storage: Subsurface Seals and Caprock Integrity** *Stéphanie Vialle, Jonathan Ajo-Franklin, and J. William Carey (Eds.)*
239 **Lithospheric Discontinuities** *Huaiyu Yuan and Barbara Romanowicz (Eds.)*

Geophysical Monograph 240

Chemostratigraphy Across Major Chronological Boundaries

Alcides N. Sial
Claudio Gaucher
Muthuvairavasamy Ramkumar
Valderez Pinto Ferreira
Editors

This Work is a co-publication of the American Geophysical Union and John Wiley and Sons, Inc.

AGU 100
ADVANCING EARTH AND SPACE SCIENCE

WILEY

This Work is a co-publication between the American Geophysical Union and John Wiley & Sons, Inc.

This edition first published 2019 by John Wiley & Sons, Inc., 111 River Street, Hoboken, NJ 07030, USA and the American Geophysical Union, 2000 Florida Avenue, N.W., Washington, D.C. 20009

Published under the aegis of the AGU Publications Committee

Brooks Hanson, Executive Vice President, Science
Lisa Tauxe, Chair, Publications Committee
For details about the American Geophysical Union visit us at www.agu.org.

Wiley Global Headquarters
111 River Street, Hoboken, NJ07030, USA

For details of our global editorial offices, customer services, and more information about Wiley products visit us at www.wiley.com.

Library of Congress Cataloging-in-Publication data is available.

ISBN: 9781119382485

Cover design: Wiley
Cover image: The Permian-Triassic boundary beds in the Ali Bashi Mountains, 9 km west of the town Julfa (East Azerbaijan province, Iran) (© Dieter Korn, February 2018)

Set in 10/12pt Times New Roman by SPi Global, Pondicherry, India

10 9 8 7 6 5 4 3 2 1

CONTENTS

Part IV: Mesozoic

Part V: Cenozoic

CONTRIBUTORS

Jhon Willy Lopes Afonso
Programa de Pós-Graduação em Geologia e Geoquímica
Faculdade de Geologia
Instituto de Geociências
Universidade do Pará
Belém, PA, Brazil

José Antonio Barbosa
LAGESE
Department of Geology
Federal University of Pernambuco
Recife, PE, Brazil

Stig M. Bergström
School of Earth Sciences
Division of Earth History
The Ohio State University
Columbus, OH, USA

Farid Chemale Junior
Programa de Pos-graduação em Geologia
Universidade Vale do Rio dos Sinos
São Leopoldo, Rio Grande do Sul, Brazil

Jiubin Chen
State Key Laboratory of Environmental Geochemistry
Institute of Geochemistry
Chinese Academy of Sciences
Guiyang, China

Simonetta Cirilli
Department of Physics and Geology
University of Perugia
Perugia, Italy

Fábio Henrique Garcia Domingos
Programa de Pós-Graduação em Geologia e Geoquímica
Faculdade de Geologia
Instituto de Geociências
Universidade do Pará
Belém, PA, Brazil

Karol Tatiana Dussan-Tapias
Universidad de Caldas
Manizales, Colombia

Valderez Pinto Ferreira
NEG–LABISE
Department of Geology
Federal University of Pernambuco
Recife, PE, Brazil

Robert Frei
Department of Geosciences and Natural Resource Management
University of Copenhagen
Copenhagen, Denmark;
Nordic Center for Earth Evolution (NordCEE)
University of Southern Denmark
Odense, Denmark

Claudio Gaucher
Instituto de Ciencias Geológicas
Facultad de Ciencias
Universidad de la República
Montevideo, Uruguay

Abbas Ghaderi
Department of Geology
Faculty of Sciences
Ferdowsi University of Mashhad
Mashhad, Iran

Nova Giovanny
Corporación Geológica Ares
Bogotá, Colombia

Daniel Goldman
Department of Geology
University of Dayton
Dayton, OH, USA

Felipe Guadagnin
Universidade Federal do Pampa
Caçapava do Sul
Rio Grande do Sul, Brazil

Stephen Peter Hesselbo
Camborne School of Mines and Environment and Sustainability Institute
University of Exeter
Cornwall, United Kingdom

Franziska Heuer
Museum für Naturkunde - Leibniz Institute for Evolution and Biodiversity Science
Berlin, Germany

John A. Higgins
Department of Geosciences
Princeton University
Princeton, NJ, USA

Alan J. Kaufman
Department of Geology
Earth System Science Interdisciplinary Center
University of Maryland
College Park, MD, USA

Dieter Korn
Museum für Naturkunde - Leibniz Institute for Evolution and Biodiversity Science
Berlin, Germany

Christoph Korte
Department of Geosciences and Natural Resource Management
University of Copenhagen
Copenhagen, Denmark

Jean Michel Lafon
Programa de Pós-Graduação em Geologia e Geoquímica
Faculdade de Geologia
Instituto de Geociências
Universidade do Pará
Belém, PA, Brazil;
Research Productivity of CNPq
Brasília, Brazil

Luis Drude Lacerda
LABOMAR, Institute of Marine Sciences
Federal University of Ceará
Fortaleza, Brazil

Ramasamy Nagarajan
Department of Applied Geology
Curtin University
Sarawak, Malaysia

Afonso César Rodrigues Nogueira
Programa de Pós-Graduação em Geologia e Geoquímica
Faculdade de Geologia
Instituto de Geociências
Universidade do Pará
Belém, PA, Brazil;
Research Productivity of CNPq
Brasília, Brazil

József Pálfy
Department of Geology
Eötvös University
Budapest, Hungary;
Research Group for Paleontology
Hungarian Academy of Sciences-Hungarian Natural History Museum-Eötvös University
Budapest, Hungary

Natan Silva Pereira
NEG–LABISE
Department of Geology
Federal University of Pernambuco
Recife, PE, Brazil;
Department of Biology
State University of Bahia
Paulo Afonso, Brazil

Roberto Vizeu Lima Pinheiro
Programa de Pós-Graduação em Geologia e Geoquímica
Faculdade de Geologia
Instituto de Geociências
Universidade do Pará
Belém, PA, Brazil

Muthuvairavasamy Ramkumar
Department of Geology
Periyar University
Salem, TN, India

Danielle Santiago Ramos
Department of Geosciences
Princeton University
Princeton, NJ, USA

Guilherme Raffaeli Romero
Programa de Pós-Graduação em Geologia e Geoquímica
Faculdade de Geologia
Instituto de Geociências
Universidade do Pará
Belém, PA, Brazil

Priyadarsi Debajyoti Roy
Instituto de Geología
Universidad Nacional Autónoma de México
Ciudad de México, México

Isaac Daniel Rudnitzki
Departamento de Geologia
Universidade Federal de Ouro Preto
Ouro Preto, MG, Brazil

Micha Ruhl
Department of Geology
Trinity College Dublin
The University of Dublin
Dublin, Ireland;
Department of Earth Sciences
University of Oxford
Oxford, United Kingdom

Evelyn Aparecida Mecenero Sanchez
Faculty of Geological Engineering
Instituto de Ciência e Tecnologia
Universidade Federal dos Vales do Jequitinhonha e Mucuri
Diamantina, MG, Brazil

Hudson Pereira Santos
Programa de Pós-Graduação em Geologia e Geoquímica
Faculdade de Geologia
Instituto de Geociências
Universidade do Pará
Belém, PA, Brazil

Iara Maria dos Santos
Programa de Pós-Graduação em Geologia e Geoquímica
Faculdade de Geologia
Instituto de Geociências
Universidade do Pará
Belém, PA, Brazil

Martin Schobben
School of Earth and Environment
University of Leeds
Leeds, United Kingdom;
Museum für Naturkunde - Leibniz Institute for Evolution and Biodiversity Science
Berlin, Germany

Alcides Nobrega Sial
NEG–LABISE
Department of Geology
Federal University of Pernambuco
Recife, PE, Brazil

José Bandeira
Programa de Pós-Graduação em Geologia e Geoquímica
Faculdade de Geologia
Instituto de Geociências
Universidade do Pará
Belém, PA, Brazil

Joelson Lima Soares
Programa de Pós-Graduação em Geologia e Geoquímica
Faculdade de Geologia
Instituto de Geociências
Universidade do Pará
Belém, PA, Brazil

Juan Carlos Silva-Tamayo
Antonio Nariño University
Bogotá, Colombia;
Tetslab Geoambiental
Medellin, Colombia

Vinod Chandra Tewari
Department of Geology
Sikkim University
Gangtok, SK, India

Melanie Tietje
Museum für Naturkunde - Leibniz Institute for Evolution and Biodiversity Science
Berlin, Germany

Clemens Vinzenz Ullmann
Camborne School of Mines and Environment and Sustainability Institute
University of Exeter
Cornwall, United Kingdom

Helmut Weissert
Department of Earth Sciences
ETH Zurich
Zurich, Switzerland

Paul B. Wignall
School of Earth and Environment
University of Leeds
Leeds, United Kingdom

PREFACE

Multiple global changes marked the major (chrono) stratigraphic boundaries in the geological history of Earth. Accordingly, these changes are documented through geochemical and stable isotopic proxies/chemostratigraphic events across the Neoproterozoic-Cambrian, Permian-Triassic, Cretaceous-Paleogene, and many other boundaries from different continents. Study of these past geological-chronological boundary records holds the key for understanding the multiple proxies and diverse consequences of these changes. This book focuses on global studies from Archean-Paleoproterozoic, Proterozoic-Paleozoic, Paleozoic-Mesozoic, and Mesozoic-Cenozoic transitions using major, trace, and platinum-group elements (PGE), REE, and elemental and stable and radiogenic isotope variations. The aim of these studies is a better understanding of causes and effects of the changes that mark these important boundaries, within the lithosphere, atmosphere, biosphere, and hydrosphere. In addition, the knowledge of past positions of continents, global sea-level changes, volcanism, and mass extinction events across these boundaries are essential clues to unravel the history of our planet.

Recent studies have demonstrated that geochemical and stable isotope changes at the end-Permian mass extinction are due to abrupt climate change induced by CO_2 emission. Catastrophic end-Permian and end-Cretaceous volcanism may have released large amounts of CO_2 and other toxic gases into the atmosphere contributing to the mass extinction at these two major boundaries. Therefore, oceanic and terrestrial records of elemental and isotope chemostratigraphy are valuable tools in establishing major tectonic and climatic changes. A global paleogeographic and paleoclimatic picture of the Earth will emerge from exploring this theme.

Chemostratigraphy, an interdisciplinary discipline, has made rapid strides and promises to provide solutions to some intriguing problems of Earth processes on microscales and global scales. This book focuses on the application of chemostratigraphy to the study of major chronostratigraphical boundaries and on how it can contribute to broaden the knowledge on these boundaries. It comprises thirteen chapters, which deal with different geological units around the world. It aims at providing a concise and updated view of major chronostratigraphical boundaries from the chemostratigraphical viewpoint, highlighting (i) chemostratigraphy as an important stratigraphical tool of wide interest, as attested by growing popularity and expanding application to many geological problems, despite the absence of textbooks on this field; (ii) it supplements other lines of evidence for analyzing and documenting geological phenomena; (iii) it is important in unraveling the intriguing nature of chronostratigraphical boundaries; (iv) it helps to make a more accurate determination of boundaries and more robust correlations; and (v) high-resolution chemostratigraphy along available biostratigraphy of these boundaries helps in determining the cause of extreme biotic turnover.

With this book, our intention is to provide students and researchers a comprehensive review of major turnovers and global changes at chronostratigraphical boundaries from the chemostratigraphic viewpoint. Thirteen chapters in this volume embody relevant issues and conclusions on nature and possible causes of the major chronostratigraphic boundaries and are grouped into five sections: In Part I, Alcides Sial and others propose that chemostratigraphy should be a formal stratigraphic method, and Mu Ramkumar and others present a glossary of chemostratigraphy, including key phrases and the terminology used in this field. Part II encompasses five chapters on the major Precambrian boundaries, while two chapters on Paleozoic chronostratigraphical boundaries are found in Part III. Four chapters cover the major Mesozoic boundaries in Part IV, and a summary on the chemostratigraphy of the most recent era of Earth's history, the Cenozoic, is found in Part V.

Claudio Gaucher and Robert Frei focus on the Archean-Proterozoic boundary (2500 Ma) and the Great Oxygenation Event, the most dramatic change on Earth's history. They discuss three different proposals for the placement of this boundary and a corresponding Global Boundary Stratotype Section and Point: (i) to keep it at 2500 Ma, aided by prominent BIF units, Mo abundance, and Mo isotopes; (ii) to place it at the base of the second Huronian glaciation (ca. 2.35–2.40 Ga), thought to represent a "snowball" event; and (iii) to use the termination of the mass-independent fractionation of sulfur and the increase in the $\delta^{34}S$ amplitude of sulfides as the main criteria.

Farid Chemale Jr. and Felipe Guadagnin review the chronochemostratigraphy of some platform sequences across the Paleoproterozoic-Mesoproterozoic boundary. The Paleoproterozoic era is known to be an interval of major changes in the Earth's atmosphere, biosphere, oceans, and lithosphere. In contrast, the Mesoproterozoic era is considered for some as a "boring interval" due to

the paucity of changes, especially in life forms. Carbonate platforms in basins of this interval exhibit essentially flat carbon isotope signature (around a mean of −0.6‰, with extreme $\delta^{13}C$ values seldom lying further than 1‰ from the mean) suggesting a stable paleoclimate, implying that the global ocean reached a state of equilibrium in the mid-Paleoproterozoic and remained stable for much of the following billion years.

Juan Carlos Silva Tamayo and others have used geochronological and C and Sr chemostratigraphic data from late Neoproterozoic to early Mesoproterozoic marine carbonate successions to propose reference $\delta^{13}C$ and $^{87}Sr/^{86}Sr$ chemostratigraphic pathways for the Mesoproterozoic-Neoproterozoic transition. While late Mesoproterozoic marine carbonates display $\delta^{13}C$ decrease from 4‰ to −2‰, carbonates across the Mesoproterozoic-Neoproterozoic transition exhibit a positive $\delta^{13}C$ shift, from −2‰ to +2‰, followed by subsequent decrease to values around −1‰. This decrease of $\delta^{13}C$ values is followed by a new increase to predominantly positive ones in the early Neoproterozoic. The reference chemostratigraphic pathways obtained also suggest that late Mesoproterozoic carbonate successions display predominantly higher $^{87}Sr/^{86}Sr$ values than early Neoproterozoic carbonates.

Afonso C. R. Nogueira and others review the status of knowledge of the Cryogenian-Ediacaran transition and focused on the southern margin of the Amazon Craton, an important area for studying evidence of Neoproterozoic glaciations. They examine four outcrops of cap carbonate that overlie Marinoan diamictites and perhaps record the best preserved boundary between Cryogenian (850–635 Ma) and Ediacaran (635–541 Ma) in South America. The new data discussed and the review of previous geological, geochemical, and isotopic information provide a robust stratigraphic framework that confirms unequivocally the record of Cryogenian-Ediacaran boundary in the Southern Amazon Craton.

Alan J. Kaufman assesses the state of knowledge of the Precambrian-Phanerozoic boundary, discussing in detail the progress in resolving several major issues of this transitional period. He also provides a review of profound changes in the carbon and sulfur cycles across this critical transition in order to better understand climatic and biological events and further proposes a novel resource-based hypothesis for the rise and fall of the Ediacaran biota.

Stig Bergström and Daniel Goldman focus on the Ordovician-Silurian interval making a comprehensive summary from C isotope chemostratigraphy and conclude that this boundary cannot be defined in terms of $\delta^{13}C$ chemostratigraphy. A comparison between biostratigraphy and chemostratigraphy indicates that the graptolite-defined base of the Silurian is located at a stratigraphic level only a little higher than the end of the Hirnantian carbon isotopic excursion (HICE).

Martin Schobben and others discuss the effect of sampling strategies on stratigraphic carbonate-carbon isotope trends using chemostratigraphy across the Permian-Triassic boundary as an example. They assess how much bed-internal carbon isotope variation of rock sequences can bias carbon isotope frameworks, as well as how much anomalous signals can be introduced to carbon isotope records by polymorph assemblages and/or microbially mediated precipitates. They propose that bulk-rock sampling strategies can improve the reliability of recording primary chemical signals.

Christoph Korte and others review the Triassic-Jurassic transition, marked by one of the biggest mass extinctions in Earth's history, coeval with early stages of the Central Atlantic magmatic province (CAMP) volcanism, showing strong perturbation of the global carbon and major fluctuations in carbon isotope ratios. Changes in magnitude and rate of change in $\delta^{13}C$, coincident with the end-Triassic mass extinction interval, differ between substrates (organics vs. calcite) and depositional environments. Thus, fluxes of carbon release at this time and links to the emplacement of CAMP are poorly understood.

Helmut Weissert reports on the Jurassic-Cretaceous carbon isotope geochemistry as a proxy for paleoceanography and tool for stratigraphy. He concludes that oceanography explains why C isotope stratigraphy may not be very useful as a tool when defining GSSP of the Jurassic-Cretaceous boundary. Alcides Sial and others made an extensive review on the Cretaceous-Paleogene boundary focusing on elemental and isotope chemostratigraphy from apparently continuous sections and testing the impact versus volcanism hypotheses using Hg chemostratigraphy and Hg isotopes.

Priyadarsi Roy and others review the geological, climatic, and paleobiotic events of the Cenozoic era using chemostratigraphic markers to identify gaps in our understanding. They suggest further subdivisions of the Cenozoic, namely, the early and late Paleocene; the early, middle, and late Eocene; the early and late Oligocene; the early, middle, and late Miocene; the Pliocene; the Pleistocene; and the Holocene. Through the review, these authors found the chemostratigraphic trends of the Cenozoic to be essentially of a continuum of Mesozoic trends.

Alcides N. Sial
Claudio Gaucher
Muthuvairavasamy Ramkumar
Valderez Pinto Ferreira

ACKNOWLEDGMENTS

This book project started with the idea of organizing a session on "Elemental and Isotopic Chemostratigraphy Across Major Chronostratigraphical Boundaries" within the framework of the 35th International Geological Congress at Cape Town, South Africa (2016). Rituparna Bose acting as books editor of the American Geophysical Union (AGU) inquired us as leaders of that session on our willingness of contributing/compiling a special volume in the form of a major reference work on a related research topic. Upon our positive reply, she formally extended us an invitation to prepare this research work to the prestigious American Geophysical Union Book Series. Technical assistance at the AGU/Wiley, especially by Kathryn Corcoran, and the editorial team at AGU are gratefully acknowledged for their professional, yet timely handling of many requests/tasks since inception of this work.

All the contributions presented in this book were reviewed by internationally renowned experts. The nature of this book required some manuscripts to be long and full of detailed information which made their reviewing a time-consuming effort. We are especially grateful to a number of active researchers and experts who shared their expertise and time and made important contributions to the success of this book by providing critical, constructive, and, in some cases, thought-provoking reviews. They are listed below in alphabetical order:

Thierry Adatte (Institute of Earth Sciences, University of Lausanne, Switzerland)

José Antônio Barbosa (Federal University of Pernambuco, Recife, Brazil)

Michael Bau (Jacobs Universität, Bremen, Germany)

Paulo Cesar Boggiani (University of São Paulo, São Paulo, Brazil)

Ana-Voica Bojar (Universitat Salzburg, Salzburg, Austria)

Zhong-Qiang Chen (China University of Geosciences, Wuhan, China)

Sean Crowe (University of British Columbia, Vancouver, Canada)

Milene Figueiredo (Center of Research and Development Leopoldo Américo Miguez de Mello, Petróleo Brasileiro S.A., Brazil)

Karl B. Föllmi (Institute of Earth Sciences, University of Lausanne, Switzerland)

Robert Frei (University of Copenhagen, Copenhagen, Denmark)

Reinhardt Adolf Fuck (University of Brasília, Brasília, Brazil)

Francesca Furlanetto (Simon Fraser University, Vancouver, British Columbia, Canada)

Leo Afraneo Hartmann (Federal University of Rio Grande do Sul, Porto Alegre, Brazil)

Jens Herrle (Goethe-Universitaet, Frankfurt am Main, Germany)

Wolfram M. Kürschner (Department of Geosciences, University of Oslo, Norway)

Aroldo Misi (Federal University of Bahia, Salvador, Bahia, Brazil)

Ramasamy Nagarajan (Curtin University, Sarawak, Malaysia)

Manoj Kumar Pandit (Department of Geology, University of Rajasthan, Jaipur, India)

Gustavo Paula-Santos (Institute of Geosciences, State University of Campinas, São Paulo, Brazil)

Gregory Price (School of Geography, Earth and Environmental Sciences, University of Plymouth, United Kingdom)

Claudio Riccomini (University of São Paulo, São Paulo, Brazil)

Priyadarsi D. Roy (National Autonomous University of Mexico, Mexico)

Isaac Rudnitzki (Federal University of Ouro Preto, Minas Gerais, Brazil)

Finn Surlyk (University of Copenhagen, Copenhagen, Denmark)

Vinod Chandra Tewari (Geology Department, Sikkim University, Sikkim, India)

Manish Tiwari (National Centre for Antarctic and Ocean Research, Vasco da Gama, Goa, India)

Paul B. Wignall (School of Earth and Environment Sciences, University of Leeds, United Kingdom)

ANS and VPF acknowledge the continuous financial support from Brazilian agencies (CNPq, FINEP, CAPES, VITAE, FACEPE) through funds to defray costs with traveling, visiting scientists, scholarships, field trips, maintenance of laboratories, and chemical and isotope analyses.

CG gratefully acknowledges continued support from the Sistema Nacional de Investigadores (SNI) (Uruguay). Involvement of MR on this subject and scientific collaboration with national and international academic and research institutions have been supported by research grants from various organizations, namely, the Alexander von Humboldt Foundation and the German Research Foundation (Germany), the University Grants Commission, the Council of Scientific and Industrial Research, the Department of Science and Technology, the Oil Industry Development Board, and the Oil and Natural Gas Corporation Limited (India), for which MR is thankful.

Part I
Introduction

1

Chemostratigraphy as a Formal Stratigraphic Method

Alcides Nobrega Sial[1], Claudio Gaucher[2], Muthuvairavasamy Ramkumar[3], and Valderez Pinto Ferreira[1]

ABSTRACT

Elemental and isotope chemostratigraphies are used as tracers for glacial events, buildup of volcanic gases during glaciations (e.g., CO_2), role of volcanism in mass extinction, salinity variation, redox state of the ocean and atmosphere, and provenance, among other applications. The use of isotope systems (C, O, S, N, Sr, Nd, Os), nontraditional stable isotope systems (e.g., Ca, Mg, B, Mo, Fe, Cr, Li), and elemental composition or elemental ratio (e.g., V, Ir, Mo, P, Ni, Cu, Hg, Rb/K, V/Cr, Zr/Ti, Li/Ca, B/Ca, Mg/Ca, I/Ca, Sr/Ca, Mn/Sr, Mo/Al, U/Mo, Th/U) in chemostratigraphy, especially across major chronological boundaries, are reviewed in this chapter. Furthermore, it is discussed what validates chemostratigraphy as a formal stratigraphic method.

1.1. INTRODUCTION

The use of elemental and isotope chemostratigraphy in interpretation and correlation of global events was established with the pioneer work of *Emiliani* [1955] on oxygen isotope composition of foraminifers from deep-sea cores. *Shackleton and Opdyke* [1973] established the first 22 oxygen isotope stages, which was effectively the first formal application of chemostratigraphy. *Williams et al*. [1988] extended the oxygen isotope stage zonation to the rest of the Quaternary and *Lisiecki and Raymo* [2005] to the whole Pliocene. The success of oxygen isotope chemostratigraphy encouraged researchers to use stable isotope stratigraphy in ancient sedimentary successions.

Precambrian chemostratigraphy followed the pioneer research by William T. Holser on ancient ocean water chemistry [*Kaufman et al*., 2007a]. Long-term fluctuations in the chemistry of the seawater have been examined from the C isotope record across thick successions [e.g., *Veizer et al.,* 1980; *Magaritz et al*., 1986], and, in spite of potential effects of late diagenesis on isotope record, important isotope events were demonstrated on a global scale [e.g., *Knoll et al.,* 1986; *Magaritz*, 1989; *Holser*, 1997]. Since then, it became evident that contemporaneous, geographically widely separated marine strata registered similar isotopic compositions. Thereafter, chemostratigraphy became an important technique/tool of intrabasinal and interbasinal stratigraphic correlation to help assemble Precambrian stratigraphic record from fragments preserved in different successions [*Kaufman et al*., 2007b; *Karhu et al.,* 2010; *Sial et al*., 2010a], compensating for poor biostratigraphic resolution of Precambrian fossils [*Veizer et al.,* 1980; *Knoll et al.,* 1986; *Magaritz et al*., 1986; *Knoll and Walter*, 1992; *Kaufman et al.,* 1997; *Corsetti and Kaufman*, 2003; *Halverson et al.,* 2005]. Correlations established through chemostratigraphy can be used to comment on biogeochemical and climate changes through time although the paucity of radiometric constraints on the absolute age of few of the extreme isotope excursions have led to debates on their temporal equivalence [e.g., *Kaufman et al.,* 1997; *Kennedy et al.,* 1998; *Calver et al.,* 2004; *Allen and Etienne*, 2008].

[1] *NEG–LABISE, Department of Geology, Federal University of Pernambuco, Recife, PE, Brazil*

[2] *Instituto de Ciencias Geológicas, Facultad de Ciencias, Universidad de la República, Montevideo, Uruguay*

[3] *Deparment of Geology, Periyar University, Salem, TN, India*

Chemostratigraphy Across Major Chronological Boundaries, Geophysical Monograph 240, First Edition.
Edited by Alcides N. Sial, Claudio Gaucher, Muthuvairavasamy Ramkumar, and Valderez Pinto Ferreira.

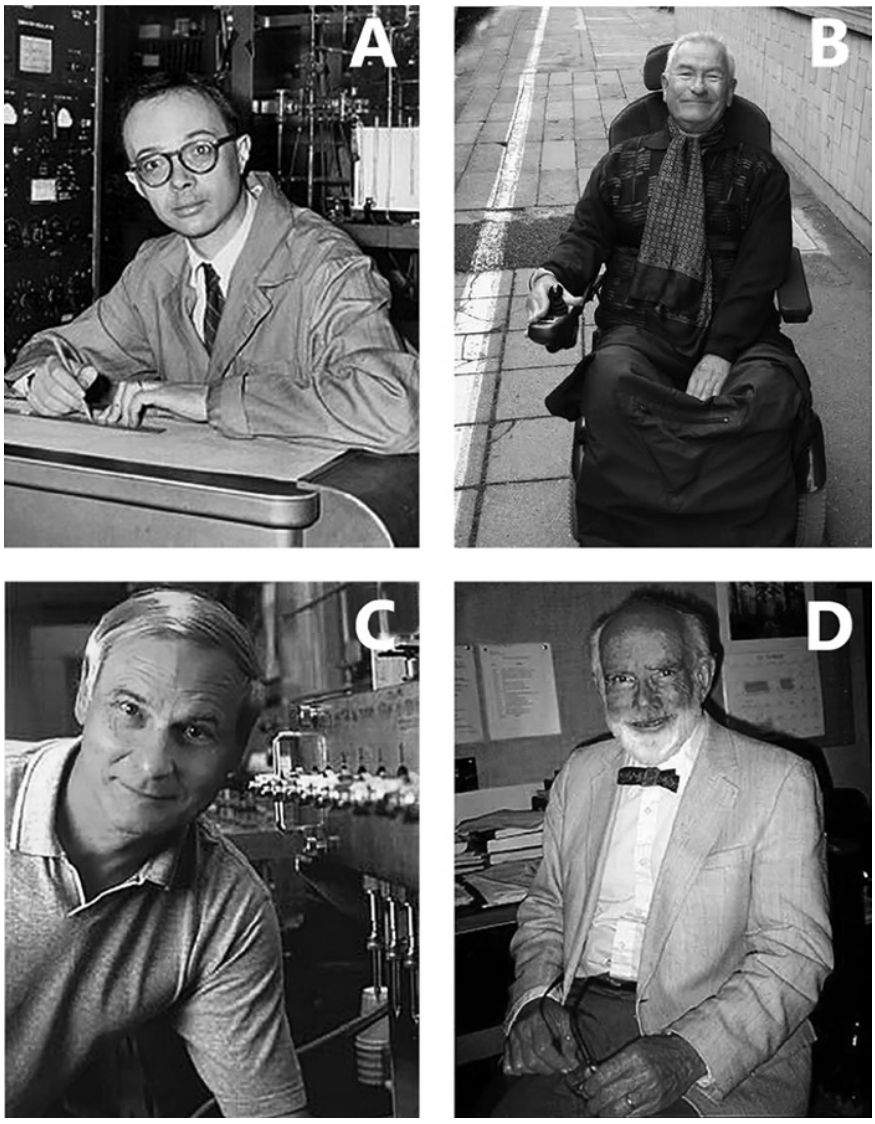

1.2. BASIS AND DEVELOPMENT OF CHEMOSTRATIGRAPHY

High-resolution chemostratigraphy provides records that are multidimensional and that may yield climatic, stratigraphic, biologic, environmental, oceanographic, and, last but not least, tectonic information. Hence, the number of studies relying on isotope stratigraphy has grown substantially. In the case of C isotope stratigraphy, it can be even applied to sedimentary rocks diagenetically altered or that have undergone up to amphibolite facies metamorphism but that may have retained the original isotope signal [*Melezhik et al.,* 2005; *Nascimento et al.,* 2007; *Kaufman et al*., 2007b; *Chiglino et al.,* 2010].

There are a myriad of isotope systems that have been successfully used in chemostratigraphy: carbon, oxygen, sulfur, nitrogen, calcium, boron, chromium, molybdenum, lithium, strontium, neodymium, osmium, iron, and zinc. In order to apply the isotope record of any of these systems for chemostratigraphy of sedimentary sequences, it is essential to have good knowledge of the secular and other variations of marine isotope ratios. As carbon isotopes have higher resilience against postdepositional alteration, they are measured in carbonates and organic matter that led to the establishment of a larger database than other isotope systems. Therefore, $\delta^{13}C$ on carbonates are more widely used in chemostratigraphy, except in carbonate-poor successions characterized by black shales [e.g., *Johnston et al.,* 2010] in which one can measure organic carbon isotopes or carbonate carbon isotopes on fossils (bivalves, ammonites, belemnites, ostracods, etc.). An attempt to compile carbon isotope data to determine a secular variation curve of $\delta^{13}C$ has revealed remarkable $\delta^{13}C$ anomalies in the Proterozoic and Phanerozoic

[e.g., *Veizer et al.,* 1980, 1999; *Karhu and Holland*, 1996; *Hoffman et al.,* 1998b; *Kah et al.,* 1999; *Melezhik et al.,* 1999, 2007; *Zachos et al.,* 2001; *Lindsay and Brasier*, 2002; *Halverson et al.,* 2005, 2010a, 2010b; *Saltzman*, 2005; *Bekker et al.,* 2006; *Saltzman and Thomas*, 2012], and it became apparent that $\delta^{13}C$ minima, perhaps, follow main extinction events [e.g., *Magaritz*, 1989]. The Hirnantian and Frasnian-Famennian episodes, however, are characterized by a positive excursion, and negative excursions are known where extinction was only minor (e.g., early Aptian). A compilation of global secular variation curves of $\delta^{13}C$, $\delta^{18}O$, $\delta^{34}S$, and $^{87}Sr/^{86}Sr$, together with major anoxic events, glaciations, and sea-level variation, can be found in *Sial et al*. [2015a].

The use of chemostratigraphy as a stratigraphic tool requires a careful examination of the diagenetic history of rocks. Petrographic, elemental (e.g., Mn/Sr, Sr, and Rb/Sr vs. $\delta^{13}C$), and isotopic ($\delta^{18}O$ vs. $\delta^{13}C$) proxies are fundamental for the assessment of the nature of C isotope signals [e.g., *Marshall*, 1992; *Jacobsen and Kaufman*, 1999; *Melezhik et al.,* 2001]. In doing so, dolostones and limestones have to be dealt with separately due to their different capacity to retain primary isotopic compositions [e.g., *Kah et al.,* 1999; *Gaucher et al.,* 2007].

Two special issues focusing Precambrian chemostratigraphy were published in *Chemical Geology* [*Kaufman et al*., 2007a] and *Precambrian Research* [*Karhu et al.,* 2010]. In these special issues, results of some cutting-edge research on traditional (C, Sr, S) isotope chemostratigraphy, few nontraditional isotope systems (Ca), and Hg chemostratigraphy have been reported. These publications encompass studies that highlighted chemical events from the Paleoproterozoic (Africa, South America, Europe, and India), Mesoproterozoic (South America), and Cryogenian-Ediacaran (North America, South America, and India) and a special focus to the atmospheric, climatic, and biogeochemical changes in both ends of the Proterozoic eon. In addition, a comprehensive synthesis on the basis and use of chemostratigraphy is presented in the book by *Ramkumar* [2015].

1.2.1. Hydrogen Isotopes

Hydrogen isotopes are relatively little used in chemostratigraphy except in studies of ice and snow stratigraphy, but deuterium has proved to be important isotope in defining the Holocene Global Stratotype Section and Point (GSSP) [*Walker et al.,* 2009]. Quaternary scientists have always sought a boundary stratotype for the Holocene in terrestrial sedimentary records, but it was within the NorthGRIP (NGRIP) ice core, Greenland, that the Holocene GSSP at 1492.45 m depth has been ratified by the International Union of Geological Sciences (IUGS). Physical and chemical parameters within the ice enable the base of the Holocene, marked by the first signs of climatic warming at the end of the Younger Dryas/Greenland Stadial 1 cold phase, located with a high degree of precision [*Walker et al.,* 2009]. This climatic event is reflected in an abrupt shift in deuterium excess values, accompanied by more gradual changes in $\delta^{18}O$, dust concentration, a range of chemical species, and annual layer thickness.

1.2.2. Carbon Isotopes

Carbon isotope investigation on Paleoproterozoic carbonate rocks of the Lomagundi province in Africa revealed much larger $\delta^{13}C$ variation [*Schidlowski et al.,* 1983] than previously known from the Phanerozoic carbonate successions [*Veizer et al.,* 1980]. This observation led to the assumption that $\delta^{13}C$ stratigraphic variation could be a tool in stratigraphic correlation. The pioneer work of *Scholle and Arthur* [1980] is one of the first to use carbon isotopes as stratigraphic tool, and *Berger and Vincent* [1981] recognized chemostratigraphy as a valid stratigraphic method. The potential use of $\delta^{13}C$ trends and excursions of marine carbonates to date and correlate rocks relies on the fact that their $^{13}C/^{12}C$ ratios varied over time as the result of partitioning of carbon between C_{org} and C_{carb} reservoirs in the lithosphere [e.g., *Shackleton and Hall*, 1984; *Berner*, 1990; *Kump and Arthur*, 1999; *Falkowski*, 2003; *Sundquist and Visser*, 2004; *Saltzman and Thomas*, 2012]. The knowledge of the C isotope record is very important not only in stratigraphic correlation but also because of its potential to help understand the development of Earth's climate, evolution of its biota, and CO_2 levels in the atmosphere.

The compilations of the secular $\delta^{13}C_{carb}$ variation for the entire Phanerozoic [*Veizer et al.,* 1999] and the Cenozoic [*Zachos et al.,* 2001] were important steps to enable carbon isotope chemostratigraphy to be routinely used as a stratigraphic tool. Currently, the most complete available curve on the $\delta^{13}C_{carb}$ fluctuations through geologic time has been compiled from multiple literature sources by *Saltzman and Thomas* [2012]. Difficulties faced in constructing such a curve reside on the fact that materials analyzed for curve construction, available in the literature, differ between authors and geological time periods, as cautioned by *Saltzman and Thomas* [2012]. In an attempt to use these compiled curves, one should carefully consider whether skeletal carbonate secreted by specific organisms or bulk carbonate has been used in evaluating or comparing C isotope stratigraphic records. Apparently, the most accepted carbonate $\delta^{13}C_{carb}$ record spanning the Neoproterozoic era is found in *Halverson et al*. [2010a, 2010b].

Covariation between $\delta^{13}C_{carb}$ and $\delta^{13}C_{org}$ helps find out whether variations in the $\delta^{13}C_{carb}$ record reflect changes in

the isotopic composition of the ancient dissolved inorganic carbon (DIC) pool [e.g., *Oehlert and Swart,* 2014]. Covariant $\delta^{13}C_{carb}$ and $\delta^{13}C_{org}$ records attest that both carbonate and organic matter were originally produced in the ocean surface waters and have retained their original $\delta^{13}C$ composition [e.g., *Korte and Kozur*, 2010; *Meyer et al.,* 2013] as no secondary process is able to shift $\delta^{13}C_{carb}$ and $\delta^{13}C_{org}$ in the same direction at the same rate [*Knoll et al.,* 1986]. Conversely, the decoupled $\delta^{13}C_{carb}$ and $\delta^{13}C_{org}$ records point to diagenetic alteration [e.g., *Grotzinger et al.,* 2011; *Meyer et al.,* 2013] or denounce that noise in the $\delta^{13}C_{org}$ record resulted from local syn-sedimentary processes [*Maloof et al.,* 2010]. One should remember, however, that the organic carbon isotope record is very much dependent on the source of the organic matter (terrestrial vs. marine) and terrestrial records may retain the secular variations known from the marine records.

Carbon isotopes can also be used as a pCO_2 proxy. Stratigraphic variation in the offset between the $\delta^{13}C_{carb}$ and $\delta^{13}C_{org}$ expressed by $\Delta^{13}C$ offers a potential tool for tracing paleo-pCO_2 change [*Kump and Arthur*, 1999; *Jarvis et al.,* 2011]. Increased burial of organic carbon leads to a fall in atmospheric pCO_2 and a positive excursion in both inorganic and organic carbon. The peak in $\delta^{13}C_{org}$ may postdate that of inorganic carbon and may be larger in magnitude, because $\Delta^{13}C$ decreases as atmospheric pCO_2 falls. This difference in response is tied to a drawdown in atmospheric pCO_2 [*Kump and Arthur*, 1999]. The "robust voice" of carbon isotopes has the potential to tell us about Earth's history [*Knauth and Kennedy*, 2009], but some postdepositional alteration of carbonate rocks may alter the story [*Bristow and Kennedy*, 2008]. However, indiscriminate use of C isotope stratigraphy to correlate Neoproterozoic carbonates ("blind dating") has been cautioned by *Frimmel* [2008, 2009, 2010] from his studies on REE+Y distribution in Neoproterozoic carbonates from different settings in Africa. These studies have raised some doubt on the usefulness of cap carbonates for stratigraphic correlation of Neoproterozoic sediment successions based on carbon isotopes. They deserve further investigation, although one can argue that rare earth elements (REEs) and DIC behave differently in seawater and are affected by diagenesis in a complete different way.

The application of carbon isotope chemostratigraphy to the study of oceanic anoxic events (OAEs) which record profound global climatic and paleoceanographic changes and disturbance of the carbon cycle, is one of the best examples of use of chemostratigraphy as a stratigraphic tool. The OAEs resulted from abrupt global warming induced by rapid influx of CO_2 into the atmosphere from volcanogenic or methanogenic sources and were accompanied by accelerated hydrological cycle, increased weathering, nutrient discharge to oceans, intensified upwelling, and increase in organic productivity [*Jenkyns*, 2010]. Nine major OAEs are known, the oldest in the Jurassic (Toarcian, called T-OAE, around 183 Ma), seven in the Cretaceous, and the youngest one in the Cenozoic (corresponding to the Paleocene-Eocene Thermal Maximum (PETM), around 55.8 Ma).

An OAE event implies very high burial rates of marine organic carbon (^{12}C), resulting in an increase in $\delta^{13}C$ values of marine and atmospheric carbon, as observed in the pronounced regionally developed positive carbon isotope excursion in $\delta^{13}C_{carb}$ across the Cenomanian-Turonian boundary [*Scholle and Arthur*, 1980]. However, the carbon isotope signatures of the early Toarcian, early Albian, and early Aptian OAEs are more complicated as signals from $\delta^{13}C_{carb}$, $\delta^{13}C_{org}$, and specific biomarkers exhibit both positive and pronounced negative excursions [*Jenkyns and Clayton*, 1986; *Herrle et al*., 2003; *Jenkyns*, 2003, 2010]. This observation suggests that besides carbon burial driving to global $\delta^{13}C$ heavier values, input of light carbon implies movement in the opposite direction.

The selection of a section at El Kef, Tunisia, to be the GSSP for the Cretaceous-Paleogene boundary (K-Pg; 66.02; *Molina et al.,* 2006, 2009), and of one at Dababiya, Egypt, to be the one for the Paleocene-Eocene boundary (PETM; 58.8 ± 0.2 Ma; *Aubry et al.,* 2007), is the best example of use of carbon isotope chemostratigraphy in boundary definition. A $\delta^{13}C$ negative shift in the section at El Kerf was one of the five marker criteria to define the K/Pg boundary, while the Paleocene-Eocene boundary was defined based on global $\delta^{13}C_{org}$ and $\delta^{13}C_{carb}$ isotope excursions (CIE).

1.2.3. Nitrogen Isotopes

The use of $\delta^{15}N$ variations in organic matter (kerogen, $\delta^{15}N_{org}$) has proved to be a valuable tool in the investigation of the evolution of the ocean chemistry, bioproductivity, and chemostratigraphic correlation, especially where biostratigraphy is of limited usefulness [*Beaumont and Robert*, 1999; *Papineau et al.,* 2005; *Algeo et al.,* 2008; *Cremonese et al.,* 2009]. Nitrogen isotope values for bulk samples ($\delta^{15}N_{bulk}$) from sections across the Ediacaran-Cambrian boundary in South China display positive values in the uppermost Ediacaran strata and strong negative shift in the Cambrian strata, especially in black shales, testifying to the changes in the biogeochemical cycle of the ancient ocean [*Cremonese et al.,* 2009, 2013, 2014]. Nitrate and nitrite are reduced to nitrogen gas by denitrification, as part of the global nitrogen cycle in modern oceans [*Algeo et al.,* 2008].

The hypothesis that transition from anoxic to oxygenated deep ocean took place at the end of the Neoproterozoic era (Neoproterozoic Oxygenation Event) is relatively well accepted [e.g., *Canfield et al.,* 2008; *Och and Shields-Zhou*, 2012]. Some of the available geochemical data for

the age interval of this transition, however, allow the interpretation of possibly full oxygenation in the early Ediacaran and preservation of deep ocean anoxia up to as late as the Early Cambrian [*Ader et al.,* 2014].

Changes in marine redox structure are related to changes in the nitrogen nutrient cycling in the global ocean, implying that $\delta^{15}N_{sed}$ probably reflects deep ocean redox transition [*Ader et al.,* 2014]. Nitrogen isotope data from Canada, Svalbard, Amazonia, and China, spanning the 750–580 Ma interval, together with other available $\delta^{15}N_{sed}$ data, show no apparent change between the Cryogenian and Ediacaran, revealing a $\delta^{15}N_{sed}$ distribution that closely resembles modern marine sediments, ranging from −4 to +11, with a $\delta^{15}N$ mode close to +4 [*Ader et al.,* 2014]. $\delta^{15}N$ data from the earlier Proterozoic show distribution relatively similar to this, but shifted slightly toward more negative $\delta^{15}N$ values and with a wider range. A possible explanation for similarity of this $\delta^{15}N$ distributions is that as in the modern ocean, nitrate (and hence O_2) was stable in most of the middle to late Neoproterozoic ocean and possibly much of the Proterozoic eon [*Ader et al.,* 2014].

Global climate over Quaternary glacial-interglacial time scales may have affected fluctuations of denitrification intensity whose rates varied over time, especially during OAEs (e.g., T-OAE; *Jenkyns et al.,* 2001). Some Upper Carboniferous black shales display C_{org}/N ratios and nitrogen isotope data that attest to fluctuations in the intensity of denitrification associated with glacially driven sea-level changes [*Algeo et al.,* 2008]. Sedimentary $\delta^{15}N$ increases during rapid sea-level rise in each cycle, with intensified denitrification, returning to background levels as sea level stabilized during the interglacial phase.

Bulk $^{15}N_{tot}$ data from early Toarcian black carbon-rich shales from British Isles and northern Italy (T-OAE; *Jenkyns et al.,* 2001, 2010) and from the Toarcian-Turonian OAE [*Jenkyns et al*., 2007] have revealed a pronounced positive $\delta^{15}N_{tot}$ excursion that broadly correlates with a relative maximum in weight percent TOC and, in some sections, with a negative $\delta^{13}C_{org}$ excursion. Perhaps, the upwelling of a partially denitrified, oxygenated water mass is the explanation for the relative enrichment of $\delta^{15}N_{tot}$, and the development of early Toarcian suboxic water masses and partial denitrification is attributed to increases in organic productivity [*Jenkyns et al.,* 2001]. A negative $\delta^{15}N_{org}$ peak to near 0‰ air/N_2 occurs at the Permian-Triassic (P-T) boundary parallel to a negative $\delta^{13}C$ excursion. It has been interpreted as the result of a diminished biomass of eukaryotic algae due to mass extinction, which were replaced by microbial N_2 fixers such as cyanobacteria [*Fio et al.,* 2010]. An analogous negative $\delta^{15}N_{org}$ and $\delta^{15}N_{bulk}$ excursion has been reported from the Ordovician-Silurian boundary [*Luo et al.,* 2016] and from the Ediacaran-Cambrian boundary [*Kikumoto et al.,* 2014]. Thus, nitrogen isotopes are valuable for the definition of major chronostratigraphic boundaries.

1.2.4. Oxygen Isotopes

Oxygen isotope chemostratigraphy has become an important tool for Mesozoic and Cenozoic stratigraphic correlation of marine sediments [e.g., *Friedrich et al.,* 2012]. For such studies, $\delta^{18}O$ is usually measured on benthic foraminifera to avoid isotopic gradient effects [e.g., *Emiliani*, 1955; *Shackleton and Opdyke*, 1973; *Lisiecki and Raymo*, 2005]. The demonstration of primary nature of $\delta^{18}O$ values in older successions, however, is often difficult, although oxygen isotopes have been successfully used in carbonates from belemnites and brachiopods and phosphates from shark teeth and conodonts [e.g., *Vennemann and Hegner*, 1998; *Joachimski and Buggisch*, 2002; *Puceat et al.,* 2003; *Price and Mutterlose*, 2004; *Bodin et al.,* 2009; *Dera et al.,* 2009; *Van de Schootbrugge et al.,* 2013].

Oxygen isotope ratios in foraminifera from deep-sea cores have shown a consistent pattern representing changes in the ocean-atmosphere system through time. *Emiliani* [1955], based on the major swings in his data, has recognized the "marine isotope stages" (MIS). *Shackleton* [1969] has subdivided Emiliani's stage 5 into lettered substages, and since then, Quaternary time is divided into marine isotope stages and substages. The MIS scheme was the first attempt to use oxygen isotope chemostratigraphy in the Quaternary. *Railsback et al*. [2015] have proposed the scheme of marine isotope substages currently in use.

A general increase from −8 to 0‰ VPDB in the Phanerozoic, punctuated by positive excursions coincident with cold intervals, has been recognized by *Veizer et al*. [1999] who have suggested that $\delta^{18}O$ analyses of carefully screened, well-preserved brachiopods and mollusks can still retain a primary signal even in Paleozoic samples. Nevertheless, similar consideration is not possible for the Precambrian due to the absence of calcified metazoans, except for the Ediacaran. $\delta^{18}O$ analyses of whole rock samples of Precambrian successions usually reflect diagenetic conditions, although primary trends have been reported in rare/limited occasions [Tahata *et al.,* 2012].

According to *Bao et al*. [2008, 2009], triple oxygen isotope evidence proved to be an important tool in the discrimination of early-Cryogenian from end-Cryogenian cap carbonates. Sulfate from ancient evaporites and barite shows variable negative ^{17}O isotope anomalies over the past 750 million years. An important difference in ^{17}O isotope anomalies of barite at top of the dolostones from the Marinoan cap carbonates (negative spike ∼ −0.70‰) suggests that by the time this mineral was precipitated, P_{CO2} was highest for the past 750 million years (CO_2 levels reached 0.01–0.08 bar during and just after ∼635 Ma glacial event; *Bao et al.,* 2008, 2009].

Oxygen isotopes of dissolved inorganic phosphate (δ^{18}Op) are a powerful stable isotope tracer for biogeochemical research, offering insights into the relative importance of different sources of phosphorus within natural ecosystems [*Davies et al.,* 2014]. Besides, the isotope fractionations alongside the metabolism of phosphorus allow δ^{18}Op to be used to better understand intracellular/extracellular reaction mechanisms that control phosphorus cycling.

An organic paleothermometer based upon the membrane lipids of mesophilic marine Thaumarchaeota, the tetraether index of lipids, with 86 carbon atoms (TEX86) has been used for over a decade when attempting to reconstruct sea surface temperatures (SSTs). This thermometer is particularly useful when other SST proxies are diagenetically altered (e.g., planktic foraminifera; *Pearson et al.,* 2007) or absent (e.g., alkenones; *Bijl et al.,* 2009).

The oldest TEX_{86} record is from the Middle Jurassic (~160Ma) and indicates relatively warm SST [*Jenkyns et al.,* 2012]. It has been also used to reconstruct SST throughout the Cenozoic era (66–0 Ma) [e.g., *Sluijs et al.,* 2009; *Zachos et al.,* 2006] and particularly to reconstruct the Eocene (55.8–34 Ma) SST. During the early Eocene, TEX_{86} values indicate warm high southern hemisphere latitude SSTs (20–25 °C) in agreement with other independently derived proxies (e.g., alkenones, Mg/Ca). During the middle and late Eocene, high southern latitude sites cooled, while the tropics remained stable and warm.

The field of clumped isotopes is concerned with how the various isotopes of carbon and oxygen are distributed in the lattice of the carbonate crystal, allowing distinction of the "isotopologues," that is, molecules of similar chemical composition but different isotopic composition [*Eiler*, 2007]. This field is concerned with measuring an isotopologue of CO_2 gas with a mass of 47, that is, where the two "heavy" rare isotopes (^{13}C and ^{18}O) are substituted in the CO_2 molecule. This is representative of the amount of "clumping" of the heavy isotopes in the crystal lattice of the carbonate. As $\Delta 47$ is measured, the amount of clumping at a known temperature can be determined [e.g., *Ghosh et al.,* 2006]. *Guo et al*. (2009b) provided a theoretical Δ_{47} calibration for a number of different mineralogies, making clumped isotopes to be one of the most promising paleothermometer for paleoclimate and diagenesis [e.g., *Eagle et al.,* 2010; *Tripati et al.,* 2010; *Petrizzo et al.,* 2014]. The great advantage is that it is unnecessary to know the oxygen isotope composition of the water with which carbonates have isotopically equilibrated. The growing interest on use of this technique is reflected in a rapid increase in the number of laboratories equipped to perform routine analyses of clumped isotope and by the organization of a series of international workshops focusing on its development and general applications.

1.2.5. Sulfur Isotopes

A secular δ^{34}S variation curve for evaporites (1.0 Ga to present) was reported by *Claypool et al*. [1980], and since then sulfur isotope chemostratigraphy has been largely used for marine evaporite sulfate, in terrains ranging from 1.0 Ga to recent. Extensive critical review on sedimentary sulfur through time and on potential use of sulfur isotopes in the investigation of time boundaries is found in *Strauss* [1997], while detailed discussion on the use of sulfur isotopes on Neoproterozoic chemostratigraphy can be found in *Halverson et al*. [2010a]. *Halverson et al*. [2010b] have subdivided Neoproterozoic sulfur isotope data into two kinds: one recording seawater sulfate ($\delta^{34}S_{sulph}$) and the other recording epigenic or authigenic pyrite ($\delta^{34}S_{pyr}$). The former is recovered from evaporites, barites, phosphorites, and carbonates (as carbonate-associated sulfate (CAS)). Fractionation that occurs during bacterial sulfate reduction (BSR) plus additional fractionation effects of reactions during oxidative recycling of sulfides is recorded by the pyrite data [*Canfield and Teske*, 1996], while the sulfur isotope data from barite, phosphorite, and CAS depict seawater sulfate ($\delta^{34}S_{sulph}$). Due to BSR, $\delta^{34}S_{pyr}$ is usually lower (lighter) than $\delta^{34}S_{sulph}$. Two important exceptions to this rule have been reported [*Ries et al.,* 2009]: (i) Archean successions usually yield similar values for pyrite and CAS, because the ocean was anoxic, and therefore BSR was negligible. (ii) Superheavy pyrites, that is, with δ^{34}S values exceeding that of coeval sulfides, occur in late Neoproterozoic successions and were interpreted as the result of very low sulfate concentrations and ferruginous conditions in the ocean and intense aerobic reoxidation of pyrite [*Ries et al.,* 2009].

Mass-independent fractionation (MIF) is observed in O, S, and Hg, linked to photochemical reactions in the atmosphere, and in the case of sulfur, it can be observed in ancient sediments [*Farquhar et al.,* 2000; *Guo et al*., 2009b] where it preserves a signal of the prevailing environmental conditions which makes sulfur isotopes as a tracer of early atmospheric oxygenation up to the formation of the ozone shield. The method implies measurements of multiple sulfur isotopes (δ^{33}S, δ^{34}S, and δ^{36}S) on CAS and sulfides. The creation and transfer of the mass-independent (MI) signature into minerals would be unlikely in an atmosphere containing abundant oxygen, constraining the Great Oxygenation Event (GOE) and the establishment of an ozone shield to sometime after 2.45 Ga ago. Prior to this time, the MI sulfur record implies that sulfate-reducing bacteria did not play a significant role in the global sulfur cycle and that the MI sulfur signal is due primarily to changes in volcanic activity [*Halevy et al.,* 2010]. After 2.3 Ga, the MIF signal disappears, attesting to the continued existence of an ozone layer since the Paleoproterozoic [*Guo et al*., 2009a].

Therefore, sulfur isotopes are important in the study of the Archean-Paleoproterozoic boundary and the fundamental biotic and environmental changes that took place during the GOE.

Biological and abiotic reactions in the sulfur biogeochemical cycle show distinctive stable isotopic fractionation and are important in regulating the Earth's surface redox state [*Pasquier et al.,* 2017]. The $\delta^{34}S$ composition of sedimentary sulfate-bearing phases reflects temporal changes in the global sulfur cycle and can be used to infer major changes in the Earth's surface environment, including rise of atmospheric oxygen.

Sulfur isotope pyrite-based records have been less explored. *Pasquier et al*. [2017] have studied Mediterranean sediments deposited over 500,000 y which exhibit stratigraphic variations >76‰ in the $\delta^{34}S$pyr data. These authors have demonstrated the relationship between the stratigraphic isotopic variation and phases of glacial-interglacial sedimentation rates. Their results suggest that the control of the sulfur isotope record can be associated with strong sea-level variations. Besides, they provided an important perspective on the origin of variability in such records and suggested that meaningful paleoenvironmental information can be derived from pyrite $\delta^{34}S$ records.

1.2.6. Calcium, Magnesium, and Boron Isotopes

Technological advances in analytical procedures and sophistication of equipment (e.g., micro-SIMS, nano-SIMS, MC-ICPMS) for few nontraditional stable isotopes, mainly Li, B, Mg, Cl, Ca, Cr, Fe, Ni, Cu, Zn, Ge, Se, Mo, Os, Hg, and Th [*Johnson et al.,* 2004; *Baskaran*, 2012; *Teng et al.,* 2017], have opened new avenues, some still to be explored in terms of isotope chemostratigraphy. In particular, Ca, Mo, and Fe have received more attention in Precambrian isotope chemostratigraphy [*Kasemann et al.,* 2005; *Arnold et al.,* 2004; *Siebert et al.,* 2003; *Johnson and Beard*, 2006; *Staubwasser et al.,* 2006, among others], and Cr isotopes have proven to be an important tool in this regard [*Frei et al.,* 2009, 2011, among others].

It is not known exactly how Ca isotopes work in modern carbonate rocks or the extension on how diagenesis affects them. A fairly updated review on the global calcium cycle is found in *Fantle and Tipper* [2014] and *Gussone et al*. [2016].

The global Ca isotope signal from end-Cryogenian carbonate successions suggests that Ca isotope chemostratigraphy can be an additional tool for the correlation of postglacial Neoproterozoic carbonate successions [*Higgins and Schrag*, 2010; *Kasemann et al.,* 2005; *Silva Tamayo et al*., 2007, 2010a, 2010b]. These authors have claimed that the Neoproterozoic Ca isotopic record is, perhaps, an archive of changes in the oceanic Ca isotopic composition.

Rapid glacier melting and significant increase in the Ca input to the ocean immediately after deglaciation, followed by progressive increase in carbonate precipitation and burial compensating for the large initial Ca input, have been depicted from Ca isotope behavior. Post-Sturtian and post-Marinoan global $\delta^{44/40}Ca$ patterns seem to differ from each other, probably because of the difference in Ca mass balance evolution among these two deglaciation events as a consequence of contrasting glacier melting regimes [*Silva Tamayo et al*., 2010a, 2010b]. This divergent behavior of the Ca isotopic evolution makes Ca isotope stratigraphy a promise, perhaps, to discriminate and correlate Neoproterozoic postglacial carbonate successions. Possibly, there is a close connection between Ca isotopic cycling in the Phanerozoic, seawater chemistry, carbonate sedimentation, and evolutionary trends [*Blättler et al.,* 2012]. MI isotope fractionation effects as observed in O, S, and Hg isotopes were not so far observed in Ca isotopes [*Gussone et al.,* 2016].

Use of magnesium isotope to understand geological phenomenon/processes has been on the rise during recent times [e.g., *Tipper et al.,* 2006a, 2006b, 2006c; *Higgins and Schrag*, 2010; *Wombacher et al.,* 2011; *Azmy et al.,* 2013; *Geske et al.,* 2015]. *Chang et al*. [2003], *Tipper et al*. [2008], and *Wombacher et al*. (2009) presented the systematics and analytical protocols in Mg isotope analyses, and accuracy of Mg isotope determination in MC-ICPMS was discussed by *Tipper et al*. [2008]. *Brenot et al*. (2008) examined the Mg isotope variability within a lithologically diverse river basin. The relationships between continental weathering, riverine influx of Mg into the oceans, and global Mg isotope budgets of modern oceans were examined by *Tipper et al*. [2006a, 2006b, 2006c]. *Higgins and Schrag* [2010] demonstrated the utility of constraining Mg cycle in marine sediments through the use of Mg isotope. As magnesium is part of the C cycle and dolomite is a major sink for Mg and a main control for $\delta^{26}Mg_{seawater}$, *Geske et al*. [2015] studied Mg isotope and suggested its use as a vital proxy. *Azmy et al*. [2013] are also of the similar opinion. Nevertheless, use of Mg isotopes in truly stratigraphic context has been scarce, for example, *Strandmann et al*. [2014] and *Pokrovsky et al*. [2011], to name a few. Despite this scarcity, the information that the Mg isotope system follows that of Sr and Ca isotopic systems [*Fantle and Tipper*, 2014] and the fact that the Mg isotopic composition of the oceans is relatively constant ($\delta^{26}Mg_{seawater} = -0.82 \pm 0.01$‰, *Foster et al.,* 2010) and Mg has a long residence time in the ocean (≈10 Myr; *Berner and Berner*, 1987; 14–16 Myr, *Lécuyer et al.,* 1990) could suggest its utility in establishing chemostratigraphic curve similar to that of Sr isotopic curve; however, the potential remains yet to be tapped and tested. It was *Galy et al*. [2002] who have reported a latitudinal gradient of Mg isotopic fractionation in

calcites of speleothems. *Li et al*. [2012] precipitated calcite in a wide range of temperature (4–45 °C) and reported a feeble gradient between $\delta^{26}Mg_{\text{calcite in solution}}$ and temperature (0.011 ± 0.002‰ $°C^{-1}$). This finding could help establish Mg isotope as a proxy to temporal trends of paleotemperature and paleolatitudinal variations.

There is fair agreement on that the aftermath of the Cryogenian glaciations has been marked by cap dolostone deposition that have followed intense continental chemical weathering. *Huang et al*. [2016] have explored the behavior of Mg isotopes to demonstrate that this was the picture in the deposition of the terminal Cryogenian-age Nantuo Formation and the overlying cap carbonate of the basal Doushantuo Formation, South China. They observed a δ^{26}Mg positive excursion, with values ranging from +0.56 to +0.95‰, in the top of the Nantuo Formation that likely resulted from an episode of intense chemical weathering. The siliciclastic component of the overlying Doushantuo cap carbonate, on the contrary, has yielded much lower δ^{26}Mg values (<+0.40‰), suggesting low-intensity chemical weathering during the cap carbonate deposition. *Huang et al*. [2016] concluded that such a behavior of Mg isotopes confirms an intense chemical weathering at the onset of deglaciation and that it has reached its maximum before the cap carbonate deposition.

There are a growing number of publications that have applied boron isotopes as a paleo-pH proxy although boron isotope analyses are complex [e.g., *Palmer et al.,* 1998; *Sanyal et al*., 2001; *Joachimski et al.,* 2005; *Hemming and Hönisch*, 2007; *Hönisch et al*., 2012; *Foster and Rae*, 2016]. A secular change in the boron isotope geochemistry of seawater over the Phanerozoic is found in *Joachimski et al*. [2005], based on the boron isotope geochemistry of brachiopod calcite.

It is known that oceanic uptake of CO_2 decreases ocean pH [*Kasemann et al.,* 2005]. Calcium and boron isotopes have been used to estimate paleoenvironmental conditions in the aftermath of the two major Neoproterozoic glaciations in Namibia. *Kasemann et al*. [2005] presented a record of Cryogenian interglacial ocean pH based on boron isotopes in marine carbonates. Their B isotope data suggest a largely constant ocean pH and no critically elevated pCO_2 throughout the older postglacial and interglacial periods. Marked ocean acidification event, in contrast, marks the younger deglaciation period and is compatible with elevated postglacial pCO_2 concentration. Negative δ^{11}B excursions in postglacial carbonates have been interpreted as an indication of temporary decrease in seawater pH.

It has been proposed that during the PETM, thousands of petagrams of carbon (Pg C) were released as methane or CO_2 into the ocean-atmosphere system for about 10 kyr, concomitant to a carbon isotope excursion, widespread dissolution of deep-sea carbonates, and global warming, leading to possible severe acidification of the ocean surface [*Penman et al.,* 2014]. Using boron-based proxies for ocean carbonate chemistry, these authors demonstrated that there is evidence for a pH drop of surface and seawater thermocline during the PETM. They have observed a decrease of 0.8‰ in δ^{11}B at the onset of the PETM event and a reduction of almost 40% in shell B/Ca, at a drill site in the North Pacific and similar trends in the South Atlantic and Equatorial Pacific, consistent with global acidification of the surface of the ocean.

1.2.7. Chromium, Iron, Molybdenum, and Thallium Isotopes

Widespread deepwater anoxia predominated in the Archean and Paleoproterozoic oceans, while the Neoproterozoic was transitional between anoxic and largely oxygenated Phanerozoic oceans. Stratified, ferruginous oceans have characterized the Archean-Paleoproterozoic and Neoproterozoic ocean chemistries, while during the Mesoproterozoic, sulfidic (euxinic) marine conditions prevailed in contrast with Phanerozoic oxygenated conditions [*Canfield et al.,* 2008]. Investigation on the Fe, Cr, and Mo isotope behavior has provided further insights into the question of surface ocean oxygenation [*Scott et al.,* 2008; *Frei et al.,* 2009].

It is well known that Cr is very sensitive to the redox state of the surface environment, oxidative weathering processes producing the oxidized hexavalent Cr. Positive isotopic fractionation of up to 5‰ accompanies the oxidation of the reduced Cr(III) on land [*Frei et al.,* 2009 and references therein]. *Lyons and Reinhard* [2009] and *Døssing et al*. [2011] have discussed in detail the isotopic systematic of the Cr cycle, including incorporation into banded iron formation (BIF). From Cr isotopes in BIFs, one can track the presence of hexavalent Cr in Precambrian oceans to understand the oxygenation history of the Earth's atmosphere-hydrosphere system [*Frei et al.,* 2009]. *Frei et al*. [2011] applied for the first time Cr isotope systematics to ancient carbonates, representing a useful tracer for climate change and for reconstructing the redox state of ancient seawater and atmosphere. Cr and C isotope curves in carbonates are virtually parallel [*Frei et al.,* 2011], and therefore, coupled δ^{13}C-δ^{53}Cr chemostratigraphy of mixed BIF/carbonate/chert successions may provide more continuous curves than C isotopes alone. This method is suitable for chemical sediments (BIF, chert, and carbonates), with low amounts of terrigenous material; otherwise Cr isotopic composition of the rock will predominate [*Frei et al.,* 2013]. Cr isotopes enabled the detection of early oxygenation pulses at 2.7 Ga [*Frei et al.,* 2009] and even at 2.95 Ga [*Crowe et al.,* 2013], long before the GOE. If one compares the δ^{53}Cr

values of BIF of different ages, Archean BIFs are the less fractionated and Neoproterozoic BIFs show the largest positive values, in accordance with the progressive oxygenation of surface environments [*Frei et al.,* 2009, 2013, 2017].

Iron (Fe) isotopes are a tool in the study of iron cycling due to its large isotopic fractionation attending to redox transformations in near-surface environment. Before the impossibility of applying the traditional stable or radiogenic isotope systems, the Fe isotope system has been largely applied to BIF [*Halverson et al.,* 2011]. Archean and Paleoproterozoic BIFs have revealed an extraordinary variability in Fe isotope compositions, from the stratigraphic [e.g., *Beard et al.,* 2003; *Johnson et al.,* 2008; *Heimann et al.,* 2010] to the mineral [e.g., *Johnson et al.,* 2003; *Frost et al.,* 2007] and microscale [e.g., *Steinhoefel et al.,* 2010]. These variations are usually ascribed to the large fractionation resulting from reduction/oxidation of Fe and the isotopic differences between mineral phases [e.g., *Johnson et al.,* 2008].

In Neoproterozoic iron formations (IF), Fe occurs almost predominantly as hematite [*Klein and Beukes*, 1993] in contrast to some Archean-Paleoproterozoic BIFs in which iron occurs as both Fe^{2+} and Fe^{3+} in a range of different minerals [*Klein and Beukes*, 1993]. Therefore, primary isotope signatures are easier to obtain from the Neoproterozoic BIFs which are usually associated with episodes of global glaciation (Rapitan-type BIF) as their Fe isotope composition reflects the chemistry of the glacial ocean [*Halverson et al.,* 2011].

The evolution of the redox state of the oceans can be also investigated using Mo concentrations in black shales [*Scott et al.,* 2008]. Its isotopic composition, in turn, allows differentiation between euxinic (i.e., sulfidic) and oxygenated environments [*Arnold et al.,* 2004]. Three oxygenation events at 2.65 Ga, ca. 2.5 Ga, and 550 Ma were recognized, with the late Paleoproterozoic and Mesoproterozoic (1.8–1.0 Ga) being characterized by euxinic conditions ("Canfield Ocean"; *Canfield*, 1998; *Arnold et al.,* 2004; *Scott et al.,* 2008). This is consistent with other proxies, such as MIF of sulfur and chromium isotopes.

High-precision measurements of thallium (Tl) isotope ratios were only made possible in the late 1990s, and, therefore, one has only limited knowledge of its isotopic behavior. Despite of their heavy masses of 203 and 205 a.m.u., it is known that thallium isotopes can be fractionated substantially in the marine environment [*Nielsen et al.,* 2017].

Thallium isotopes have been applied to investigate paleoceanographic processes in the Cenozoic, and a compilation of the Tl ($\varepsilon^{205}Tl_{sw}$) isotope composition of seawater over the last 75 Myrs is found in *Nielsen et al*. [2009, 2017], together with contemporaneous $\delta^{34}S_{sw}$ variation curve. These two curves show relatively similar behavior, with the lowest values within the 55–70 Ma range, the $\delta^{34}S_{sw}$ curve displaying minimum values around 55 Ma and $\varepsilon^{205}Tl_{sw}$ around 66 Ma. Thallium isotopes may be utilized as a proxy for changes in Fe and Mn supply to the water column over million year time scales according to *Nielsen and Rehkämper* [2012] to monitor changes in marine Mn sources and/or Mn oxide precipitation rates back in time.

1.2.8. Strontium and Neodymium Isotopes

As $^{87}Sr/^{86}Sr$ ratios and $\delta^{13}C$ fluctuate independently from each other, their combined use through the application of high-resolution chemostratigraphy represents a powerful tool to resolve geological problems. The radiogenic nature of ^{87}Sr, which forms as a result of radioactive decay of ^{87}Rb, implies that the $^{87}Sr/^{86}Sr$ ratio of the mantle, crust, and surface environments rises with time [e.g., *Shields,* 2007a, 2007b]. The $^{87}Sr/^{86}Sr$ seawater variation curve is better known for the Phanerozoic [e.g., *Burke et al.,* 1982; *Veizer et al.,* 1999; *McArthur et al.,* 2001; *Leckie et al.,* 2002; *McArthur*, 2010] showing long-term variations of about 500–550 Ma from the Upper Cambrian (0.709; *Montañez et al.,* 2000) gradually decreasing with a nadir of 0.7068 at 250 Ma and rising again to values of 0.7092 in the present-day ocean [*Macdougall*, 1991; *McArthur et al.,* 2001]. This makes Sr isotopes a pretty straightforward and precise method for dating marine carbonates and calcareous fossils in the upper half of the Cenozoic, for example, because $^{87}Sr/^{86}Sr$ ratios rise continuously from 0.7077 in the Bartonian (ca. 40 Ma) to 0.7092 in the Holocene [*McArthur et al.,* 2001]. Sr isotope chemostratigraphy is equally well feasible in the other periods of the Phanerozoic, depending on the morphology of the Sr isotope record. The close correlation in time between the strontium isotope excursions and the major OAEs (Jurassic and Cretaceous) is compatible with a causal linkage [e.g., *Jones and Jenkyns*, 2001].

The main source of ^{87}Sr is the weathering of Rb-rich granitic rocks. Hydrothermal vents near mid-ocean ridges are enriched in non-radiogenic ^{86}Sr [*Shields*, 2007a], and therefore, high $^{87}Sr/^{86}Sr$ ratios are considered as an indication of periods of enhanced orogenesis, while low ratios characterize periods of continental breakup and enhanced hydrothermal activity. *Flament et al*. [2011], however, have pointed out that $^{87}Sr/^{86}Sr$ is influenced by the area of emerged land rather than by orogenic processes alone, something especially important for calculations of continental growth in the Archean, when maybe <4% of Earth's area was emerged [*Shields*, 2007b; *Flament et al.,* 2011].

Efforts to compile Sr isotope data aimed at determining the secular $^{87}Sr/^{86}Sr$ seawater curve for the Proterozoic have been made [e.g., *Jacobsen and Kaufman*, 1999;

Melezhik et al., 2001; *Halverson et al*., 2007, 2010a, 2010b; *Kuznetsov et al.,* 2010]. The use of strontium isotopes in chemostratigraphy, however, is limited by the paucity of limestone in many successions. Another difficulty is posed by the likelihood of alteration in samples with low strontium contents through the incorporation of ^{87}Sr from the decay of ^{87}Rb in coexisting clay minerals [*Kaufman et al.,* 2009]. Therefore, it is advisable to consider only analyses of high-Sr limestones, less prone to postdepositional alteration. Geochemical screens (Rb/Sr, Mn/Sr, Sr concentration, and $\delta^{18}O$) have been widely adopted to evaluate the degree of postdepositional alteration of strontium isotope ratios [*Veizer et al.,* 1983; *Kaufman et al*., 1992, 1993; *Marshall*, 1992; *Jacobsen and Kaufman*, 1999; *Melezhik et al.,* 2001]. Dolostones are usually not suitable for Sr isotope studies due to the lower Sr concentrations of usually a few tens of ppm [*Kah et al.,* 1999; *Gaucher et al.,* 2007], although a few exceptions have been reported [*Sawaki et al.,* 2010].

Another problem of the method is the differing laboratory procedures, which yield different results for the same samples. The use of pre-leaching with ammonium acetate removes adsorbed Sr and yields lower $^{87}Sr/^{86}Sr$ ratios than a more aggressive one-step HCl leaching method [*Melezhik et al.,* 2001; *Rodler et al.,* 2017]. An intermediate approach for limestones is the use of 0.5 M acetic acid for a short time (5–10 min), which predominantly liberates calcite-associated Sr, thereby yielding lower Sr isotope ratios [e.g., *Frei et al.,* 2011].

Details on the neodymium isotope geochemistry are found in *DePaolo* [1988]. A "global average" εNd curve for the oceans since 800 Ma has been constructed [*Keto and Jacobsen*, 1988; *Macdougall*, 1991], although neodymium isotopes have been seldom used as a chemostratigraphic tool. Similar to Sr isotope secular curve, this curve shows ε_{Nd} values at the end of the Precambrian oceans not substantially different from those at present ones. There is a remarkable decrease of the average ε_{Nd} values (−5 to −15) in the time interval between 700 and 550 Ma. Despite the precision of modern instruments, the scatter in measured values is substantial, limiting the use of ε_{Nd} in chemostratigraphic studies. Even so, secular ε_{Nd} variations coupled with $\delta^{13}C$ and $\delta^{53}Cr$ have been reported from Ediacaran rocks from Uruguay [*Frei et al.,* 2011, 2013] and Brazil [*Dantas et al.,* 2009], yielding valuable information regarding the tectonic evolution of the basin.

1.2.9. Osmium and Lithium Isotopes

The temporal variations of the $^{187}Os/^{188}Os$ ratio are preserved in several marine depositional environments, where osmium is an ultra trace element [*Peckeur-Ehrenbrink and Ravizza,* 2000]. Several developments over the last three decades have allowed direct measuring of $^{187}Os/^{188}Os$ ratio and osmium concentration in seawater, river water, and rain, improving the knowledge on the surficial cycle of osmium [*Sharma et al.,* 1997; *Peckeur-Ehrenbrink and Ravizza,* 2000]. *Ravizza and Peucker-Ehrenbrink* [2003] have observed a decline of about 25% in the marine $^{187}Os/^{188}Os$ record that predated the Cretaceous-Paleocene transition (K-Pg) and that coincides with a warming in the late Maastrichtian. They have interpreted this osmium isotope ratio decline as a chemostratigraphic marker of the Deccan volcanism which was responsible for a transient global warming event (3–5 °C) and likely one of the causes of the K-Pg mass extinction.

Precambrian-to-Pleistocene marine osmium isotope records, particularly the Cenozoic and Mesozoic ones, and interpretations of their temporal variations have been reviewed by *Peckeur-Ehrenbrink and Ravizza* [2012]. Although the Cenozoic seawater $^{187}Os/^{188}Os$ mimics the marine $^{87}Sr/^{86}Sr$ record and suggests that both reflect continental weathering linked to climatic or tectonic processes, these two marine isotope systems differ fundamentally from each other [*Peckeur-Ehrenbrink and Ravizza,* 2000]. The marine residence time of osmium is distinctly shorter, allowing to record short-term fluctuations (e.g., glacial-interglacial periods), something that escapes to the buffered marine strontium isotope system. This difference between these two systems allows discrimination between climatic and tectonic forcings. Besides, large-amplitude changes in the marine $^{187}Os/^{188}Os$ record can be useful as chemostratigraphic event markers [*Peckeur-Ehrenbrink and Ravizza,* 2012].

The decline of atmospheric CO_2 has a potential role in initiating glaciation and its increase of terminating it [*Vandenbroucke et al.,* 2010]. Both cases involve changes in silicate weathering rates [*Lenton et al.,* 2012; *Ghienne et al.,* 2014]. The change of $^{187}Os/^{188}Os$ ratios during glacial periods may represent a response to change in silicate weathering, but does not help in tracing the weathering rate or processes involved [*Finlay et al.,* 2010]. The behavior of Li isotopes, however, is solely controlled by silicate weathering processes and, therefore, gives a unique insight into CO_2 drawdown and climate stabilization [*Pogge von Strandmann et al.,* 2017].

Biological processes do not lead to lithium isotope fractionation [*Pogge von Strandmann et al.,* 2017], and carbonate weathering does not affect Li isotope signals [*Dellinger et al*., 2017]. The δ^7Li of primary silicate rocks have a narrow range [*Sauzeat et al.,* 2015] if compared to the high variability of modern rivers which reflects weathering processes, particularly the extent of preferential uptake of ^6Li into secondary minerals [*Dellinger et al*., 2017]. Marine carbonates have a negligible sink of Li [*Marriott et al.,* 2004; *Pogge von Strandmann et al.,* 2013].

A comprehensive review on lithium isotope geochemistry is found in *Tomascak et al*. [2016] and *Penniston-Dorland*

et al. [2017] in which the possibility of use of Li isotope in chemostratigraphy has been overlooked. Lithium isotope chemostratigraphy of Late Ordovician bulk carbonate sections and brachiopods in Anticosti Island, Canada [*Achab et al.,* 2013] (Pointe Laframboise Ellis Bay West), and of an equivalent shale section at Dob's Linn, United Kingdom [*Finlay et al.,* 2010; *Melchin et al.,* 2013], was presented by *Pogge von Strandmann et al*. [2017]. In all sections in that study, the relative timings of δ^7Li and the Hirnantian carbon isotope excursion (HICE) are similar, suggesting that Li isotope excursions occur contemporaneously, consistent with the Li residence time in the ocean (1 Myr). The positive δ^7Li excursion during the Hirnantian cooling event compares well to negative δ^7Li during warming events [*Pogge von Strandmann et al.,* 2013; *Lechler et al.,* 2015].

1.2.10. Elemental Chemostratigraphy

Elemental chemostratigraphy (element and element ratios) is a supplementary, useful tool in stratigraphy, and Mo, Ir, V, Ni, Cu, P, Hg, REEs, and Fe are among the most used elements, while Mo/Al, U/Mo, Rb/K, V/Cr, Zr/Ti, I/Ca, Li/Ca, B/Ca, Sr/Ca, Mg/Ca, Mo/Th, V/Th, and Th/U ratios seem to be particularly interesting. Paleoceanographic applications of trace-metal concentration data have been reviewed by *Algeo and Rowe* [2012].

Iron speciation has been widely used to determine the redox state of ancient basins. The method involves sequential extraction procedures to extract highly reactive iron (oxide, carbonates, and sulfide) and compare their concentration to total iron (Fe_{HR}/Fe_T; *Canfield*, 1989; *Shen et al.,* 2003; *Poulton and Canfield*, 2005). Sediments deposited in an oxygenated water column yield Fe_{HR}/Fe_T lower than 0.38 [*Canfield*, 1989]. Furthermore, the sulfide-bound iron (Fe_P) can be compared to highly reactive iron (Fe_P/Fe_{HR}), with values higher than 0.8 characterizing sulfidic (euxinic) basins [*Canfield et al.,* 2008]. Iron speciation chemostratigraphy has been applied successfully to sedimentary units of different ages, from the Archean to recent [e.g., *Shen et al.,* 2003; *Poulton et al.,* 2004; *Canfield et al.,* 2008; *Lyons et al.,* 2009; *Johnston et al.,* 2010; *Scott et al.,* 2011; *Hammarlund et al.,* 2012; *Frei et al.,* 2013].

In sediments deposited immediately after major glacial events, Hg tends to concentrate as a result from leaching of volcanogenic Hg from land surface and accumulation along argillaceous sediments [*Santos et al.,* 2001]. This element is usually found in low geological background concentrations, and this makes this trace element suitable for identifying accumulation pulses in sediments that can be tentatively related to weathering processes and thus to climatic changes.

Carbon dioxide buildup in the atmosphere during the Neoproterozoic glacial events resulted from volcanism that led to enhanced greenhouse effect, ice melting, and cap carbonate deposition [e.g., *Hoffman et al.,* 1998a; *Hoffman*, 2011]. Besides, intense volcanism may have witnessed the P-T and Cretaceous-Paleogene transition (K-Pg) and was, perhaps, co-responsible for dramatic climatic changes and thus for the decrease in biodiversity and mass extinction [e.g., *Keller*, 2005; *Archibald et al*., 2010]. *Sial et al*. [2010b] demonstrated the use of Hg chemostratigraphy of the cap carbonates to document intense volcanism and resultant CO_2 buildup in the atmosphere, following the Neoproterozoic snowball events. Moreover, Hg chemostratigraphy was applied to investigate the relationships between large igneous province (LIP) activity, abrupt environmental changes, and mass extinctions [e.g., *Nascimento-Silva et al.,* 2011, 2013; *Sanei et al.,* 2012; *Sial et al*., 2013a, 2014, 2016, 2017, this volume; *Adatte et al.,* 2015; *Grasby et al.,* 2013, 2015, 2017; *Percival et al.,* 2015, 2017; *Font et al.,* 2016, 2018; *Thibodeau et al.,* 2016; *Charbonnier et al.,* 2017; *Jones et al.,* 2017; *Thibodeau and Bergquist*, 2017; *Keller et al.,* 2018). To assure that the measured Hg contents result from true Hg loading to the environment, it is necessary to examine Hg/TOC ratios for chemostratigraphy [e.g., *Grasby et al.,* 2015; *Percival et al.,* 2015]. Mercury enrichments in sedimentary successions that recorded the mid-Cenomanian Event and Oceanic Anoxic Event 2 (OAE2) in the Late Cretaceous have been regarded by *Scaife et al*. [2017] as a marker for submarine LIP volcanism, and Hg enrichment recorded in the PETM is assumed to be related to volcanic activity of the North Atlantic Igneous Province (NAIP) (e.g., *Keller et al.,* 2018). Hg is doubtless a good benchmark for high volcanic activity, but normalization by TOC is in some cases problematic if TOC values are <0.2, leading to exaggerated peaks.

Mo and V chemostratigraphy may be useful in the investigation of the redox state of deep ocean water. Mo is a redox-sensitive element, scavenged from seawater into sediments in the form of $MoSxO_{4-}x^{2-}$, under anoxic conditions [*Wen et al.,* 2015]. The transfer of aqueous Mo to the sediment can be increased by means of metal-oxyhydroxide particulate shuttles, but aqueous U is not affected by this process [*Tribovillard et al.,* 2012]. Therefore, an increase in U/Mo ratio may suggest oxic conditions [e.g., *Sosa-Montes et al.,* 2017]. According to *Scheffler et al*. [2003], certain elemental ratios can be useful as proxies for investigation of salinity variation (Rb/K), redox state (V/Cr), or provenance (Zr/Ti). Mo and V can be normalized with Th (Mo/Th and V/Th) and, together with other redox-sensitive trace elements such as Ni, Zn, and Pb, can be used to determine redox variations in ancient sedimentary successions [*Spangenberg et al.,* 2014].

REE has been extensively used in different types of sedimentary rocks, often in combination with yttrium (REEY). The most widely used proxies are Ce, Eu, and Pr

anomalies (Ce/Ce*, Eu/Eu*, Pr/Pr*), Y/Ho, La/Yb, and ΣREE, which can be applied to shales, carbonates, BIF, cherts, phosphorites, and other fine-grained rocks [*Elderfield and Greaves*, 1982; *Liu et al.,* 1988; *Bau and Dulski*, 1996; *Kato et al.,* 2006; *Lawrence and Kamber*, 2006; see *Sial et al.,* 2015b for an overview of proxies]. REE chemostratigraphy has been applied to Archean [*Kamber et al.,* 2014], Paleoproterozoic [*Bau and Dulski*, 1996], Mesoproterozoic [*Azmy et al.,* 2009], Neoproterozoic [*Tribovillard et al*., 2006; *Frimmel*, 2009; *Sansjofre et al.,* 2014; *Spangenberg et al.,* 2014; *Gaucher et al.,* 2015; *Sial et al.,* 2015b; *Hu et al.,* 2016; *Rodler et al.,* 2016], and Phanerozoic successions [*Schmitz et al.,* 1988; *Lécuyer et al.,* 2004; *Fio et al.,* 2010].

The redox behavior of iodine is well known [*Broecker et al.,* 1982]. Besides, it is also known that there is a linear covariation between carbonate-associated iodine (CAI) and IO_3^- during calcite precipitation, but I^- is completely excluded [*Lu et al.,* 2010]. This trait, coupled with the residence time of iodine in seawater (300 ky; *Broecker et al.,* 1982) and concentration near 450 nM in modern ocean, makes I/Ca (or I/Ca + Mg) ratios in carbonates a robust indicator of the presence of IO_3^- and hence oxygen in the water column. Therefore, surface ocean oxygenation has been investigated using I/Ca ratios as a paleoredox indicator [e.g., *Hardisty et al.,* 2014].

Li/Ca and B/Ca in carbonates are regarded as proxies for carbonate saturation state [*Hall and Chan*, 2004; *Hall et al.,* 2005; *Lear and Rosenthal*, 2006; *Yu and Elderfield,* 2007; *Foster*, 2008], and Mg/Ca ratios of foraminiferal shells have been regarded as useful paleothermometer to determine ocean temperature. The difference in the Mg/Ca ratio of the foraminiferal shell and that from a baseline value (defined by the global ocean Mg and Ca concentration) when calibrated for the vital effects of the organism is a function of temperature [e.g., *Lea et al.,* 2000; *Lear et al*., 2000]. The baseline composition of seawater is relatively simple to infer, once both Mg and Ca have long residence times in the oceans (>1 Ma) and are major components of ocean salts.

1.3. CHEMOSTRATIGRAPHY AND CHRONOSTRATIGRAPHIC BOUNDARIES

The International Commission on Stratigraphy (ICS) recognizes the existence of one hundred fourteen chronostratigraphic boundaries. Sixty-seven sections straddling chronostratigraphic boundaries were internationally agreed upon as reference points to define the lower boundaries of stages on the geologic time scale, the Global Boundary Stratotype Section and Point (GSSP), and a golden spike is placed precisely at the boundary defined. Accessibility and degree of representativity of the same boundary on sections worldwide are among the most important criteria in the GSSP selection. Since GSSPs require well-preserved sections of rock without interruptions in sedimentation, and since most are defined by different biozones, defining them becomes more difficult as one goes further back in time in the Precambrian.

So far, chemostratigraphy has been overlooked as a formal criterion on GSSP selection. Carbon isotope excursions (CIE) have been reported only from seven of the established GSSPs [*Cooper et al.,* 2001; *Dupuis et al.,* 2003; *Peng et al.,* 2004; *Knoll et al.,* 2006; *Xu et al.,* 2006; *Aubry et al.,* 2007; *Goldman et al.,* 2007; *Schmitz et al.,* 2011; *Keller et al.,* 2018], probably due to the absence of carbonate rocks in several chronostratigraphic boundary sections. Only in the selection of the Cretaceous-Paleogene (K-Pg; *Molina et al.,* 2006, 2009) and the Paleocene-Eocene (PETM; *Aubry et al.,* 2007) GSSPs was carbon isotope chemostratigraphy one of the criteria, and hydrogen isotopes in the Pleistocene–Holocene GSSP [*Walker et al.,* 2009]. In addition, oxygen isotopes have been reported from two other GSSPs [*Steininger et al.,* 1997; *Hilgen et al.,* 2009]. Heavy element (e.g., Ir, Os, Hg) enrichments at the Cretaceous-Tertiary boundary are well known since the seminal paper of *Alvarez et al*. [1980] and later studies [e.g., *Schmitz et al.,* 1988; *Frei and Frei*, 2002; *Sial et al.,* 2016; *Keller et al.,* 2018, and references therein].

1.4. CHEMOSTRATIGRAPHY AS FORMAL STRATIGRAPHIC METHOD

The stratigraphic record shows changes of the concentration of certain elements with time [*Morante et al.,* 1994], as a function of geological conditions including, but not limited to, tectonic, climatic, redox, oceanographic, biotic, and other processes. Chemostratigraphy enables not only apparently uniform thick successions to be subdivided and correlated with coeval strata located elsewhere [*Ramkumar*, 1999] but also thinner and more heterogeneous sedimentary records. Initially, chemostratigraphy was applied to recognize unique geochemical compositions for characterizing depositional units and correlating them with coeval strata elsewhere and found its use in the stratigraphic location of boundaries and later expanded to examination of specific causes to the stratigraphic variations of geochemical compositions [*Ramkumar et al.,* 2010, 2011]. The utility of chemostratigraphy for age determination was demonstrated through documentation of stratigraphic variations of isotopic trends, beginning with oxygen isotopes. Linear, secular, cyclic, and perturbed trends have been recognized, which are utilized for stratigraphic classification and spatial correlation [e.g., *Zachos et al.,* 2001; *Ramkumar*, 2014, 2015]. In addition, the chemozones, calibrated with absolute time, are in use as chemochrons. Although chemostratigraphy is firmly recognized as a